E.M.M. Ibrahim^a

https://doi.org/10.21608/sjsci.2025.418761.1306

AC conductivity and optical properties of In₂S₃ thin films synthesized by thermal evaporation technique

Bosy Yassin,^{a*} Mohamed Khairy,^b Amr Attia Abuelwafa,^c Moumen Samir Kamel,^a E. Kh Shokr,^a Mohamed B. Zahran,^{d,e}

Received: 2nd September 2025 Revised: 6th October 2025 Accepted: 7th October 2025

Published online: 14th November 2025

Abstract: Indium sulfide (In_2S_3) thin films were successfully deposited on glass substrate using the thermal evaporation technique. The structural, optical, electrical, and dielectric properties of the films were systematically investigated. X-ray diffraction and FE-SEM analyses confirmed the amorphous nature of the films with nanometric particle sizes and uniform surface morphology. Optical measurements revealed a high transmittance (>90%) and a direct optical band gap of 2.34 ± 0.00468 eV, slightly larger than the bulk value, likely due to quantum confinement effects. The Urbach energy was estimated to be 0.41 ± 0.0036 eV, indicating a high density of localized states. AC conductivity measurements were performed over a frequency range of 100 kHz to 8 MHz and temperature range of 303-373 K, showed two distinct conduction regions. The frequency-dependent behavior at higher frequencies followed Jonscher's universal power law, and the conduction mechanism was found to be consistent with the correlated barrier hopping (CBH) model, the activation energy was obtained to be $0.076 \pm 0.0023 \text{ev}$. Dielectric studies demonstrated strong temperature and frequency dependence of both real and imaginary permittivity components, highlighting the role of space charge and rotational dipolar polarization. The combined findings underscore the potential of thermally evaporated In_2S_3 thin films for optoelectronic and dielectric applications.

Keywords: Indium sulfide; optical properties; electrical properties; dielectric constant; solar cell; photovoltaic.

1. Introduction

Indium sulfide (In₂S₃) is one of the most promising materials used for thin film solar cell fabrication in recent times[1].In₂S₃ is a direct band gap semiconductor with n-type conductivity and non-toxic constituents[2]. The chemical stability, high visibleregion transparency, and photoconductive properties of In₂S₃ render it a superior alternative to the conventional, toxic buffer layer of cadmium sulfide[3]. Indium sulfide is found to crystallize into three different crystallographic phases: defective cubic structure (α-In₂S₃), defective spinel structure (β-In₂S₃), and layered hexagonal structure (γ-In₂S₃)[4].Among the different crystalline forms of In₂S₃, the β-phase is the most stable from room temperature up to about 420 °C. Above this temperature, β- In₂S₃ undergoes a structural transition to the αphase, which remains stable up to approximately 750 °C, while the y-phase adopts a stable trigonal crystal structure between 750 °C and the melting point (≈ 1090 °C). The β -In₂S₃ phase exhibits a high density of vacancies and a structure that provides sufficient interstitial space for doping and tuning its physical properties. Owing to these features, the β-phase is the most

stable and widely employed form of In_2S_3 in optoelectronic applications[5] and crystallizes in a normal spinel structure with a high degree of tetrahedral and octahedral vacancy sites [6][7] . Several methods have been reported for synthesizing In_2S_3 thin films namely, thermal evaporation[8] [9], RF sputtering [10], chemical bath deposition[11], spray pyrolysis[11], coevaporation [12] and electrodeposition[13]. Among these methods, thermal evaporation has gained considerable attention due to its straightforward process that does not necessitate complex instrumentation, its cost-effectiveness, and its ability to produce highly uniform smooth films[14].

In the present work, In_2S_3 thin films were grown by thermal evaporation on glass substrate. While In_2S_3 thin films have attracted considerable attention due to their promising optoelectronic properties, detailed investigations into their alternating current (AC) conductivity characteristics are still relatively limited. This highlights the need for further studies particularly under varying temperature and frequency conditions. For instance, Sankir et al. reported the properties of silver doped In_2S_3 films prepared by spray pyrolysis[15], Abassi et al. studied the Ac conductivity of β - In_2S_3 thin films, concluding that conduction mechanism is dominated by the

^aPhysics department, Faculty of science, Sohag University, Sohag 82524, Egypt

^bChemistry Department, Faculty of Science, Sohag University, Sohag, 82524, Egypt

^cNano & Thin film lab. Physics Department, Faculty of Science, South Valley University, Qena 83523, Egypt

^dJoint national Egyptian-Chinese Renewable energy laboratory, Sohag, Egypt.

^ePV Dep. Electronic institute Nozha elgedida, Cairo, Egypt.

^{*}Email: bosy abdelhady post@science.sohag.edu

Research Article

correlated barrier hopping (CBH) model at low frequencies($\leq 10^4\,\mathrm{Hz}$), while the small polaron tunneling (SPT) mechanism dominates at higher frequencies [16]. and Seyam et al. reported the ac conductivity and dielectric properties of stoichiometric $\mathrm{In_2S_3}$ thin films prepared by thermal evaporation. their study revealed that the AC conductivity follows the Jonscher's universal power law, with the frequency exponent factor s decreases as temperature increases, in agreement with correlated barrier hopping (CBH) model. Furthermore, the impedance Z, the capacitance C, the loss angle (tan δ) and the dielectric constants were also estimated at different frequencies, temperatures and thicknesses[17].

In this work, In_2S_3 thin films were grown on glass substrates using thermal evaporation technique. We have studied the optical properties, the frequency dependence of ac conductivity and dielectric parameters $\epsilon'(\omega)$ and $\epsilon''(\omega)$ at different temperatures (293K -353K) over a frequency range of (100 kHz to 8 MHz). Although the dielectric measurement is considered a proper tool for determining the electric properties and testing the feasibility of using the thin films as a buffer layer in solar cells, there is a lack of studies that focus on the dielectric properties of In_2S_3 thin films deposited on glass substrates. The obtained findings underscore the potential of In_2S_3 as a promising candidate for using as a buffer layer in advanced thin-film applications in solar energy technologies.

2. Materials and methods

In₂S₃ films were deposited by thermal evaporation technique. The deposition was carried on ultrasonically cleaned glass substrates. In₂S₃ powder (Sigma Aldrich 99.999%) was used as a source material for the thin film deposition. The chamber pressure during the deposition was maintained at 6×10⁻¹ ⁵ mbar and the source was kept 15 cm away from the substrate. The deposition rate (5 Å/sec) and thickness (~ 200 nm) of the films were recorded using the digital film thickness monitor model (SQM-160) with proven INFICON quartz crystal sensor (6 MH- with gold electrodes) by the well-established crystal microbalance method. The structural characteristics of films were carried out using the X-ray diffractometer, Bruker D8 Advance, with Cu- K_{α} radiation source ($\lambda = 1.5406$ Å). The optical characteristics were analyzed by a computer Japan) double programmable (Jasco V570, spectrophotometer (with photometric accuracy of $\pm 0.002 - 0.004$ absorbance and $\pm 0.3\%$ transmittance) over the wavelength range 500 - 2500 nm (UV-VIS-NIR) at normal incidence through a scan speed of 400 nm/min. The AC conductivity was measured as a function of frequency (in the range of 100 kHz to 8MHz) and temperature (in the range of 303-373 K) using IM 3536 LCR Meter HIOKI.

3. Results and Discussion:

3.1. Structural properties

The crystal structure of In_2S_3 thin film was carried out by using XRD. Fig.1.a shows the XRD pattern of In_2S_3 film grown on glass substrate. The film exhibits an amorphous nature, as no diffraction lines corresponding to free elements ordinary crystalline phases are detected. Nevertheless, the XRD pattern exhibits two wide peaks at 2θ =28°, which can be attributed to

short-range atomic order, indicating formation of In₂S₃ phase in the film under study. The field emission-scanning electron microscope (FE-SEM) investigation confirmed the deposition of In₂S₃ thin film on the glass substrate. The deposited In₂S₃ particles are uniformly distributed on the substrate surface as shown in the FE-SEM image depicted (Fig.1c). FE-SEM imaging at higher magnification (Fig.1d), shows that the particle size of the deposited thin film is in nanometric scale. However, the low conductivity of the deposited thin film due to the amorphous nature doesn't allow the determination of an exact value of the average particle size or configurating the particle size distribution. The EDX spectrum illustrated in Fig.1b exhibits a peak at 1.74 eV with a very high intensity, assigned to the Si coming from the substrate. In and S peaks are observed on the EDX spectrum but with a slight deviation from the stoichiometry due to the difference between the vapor pressures of sulfur and indium elements that makes differences in the evaporation rate from the starting material.

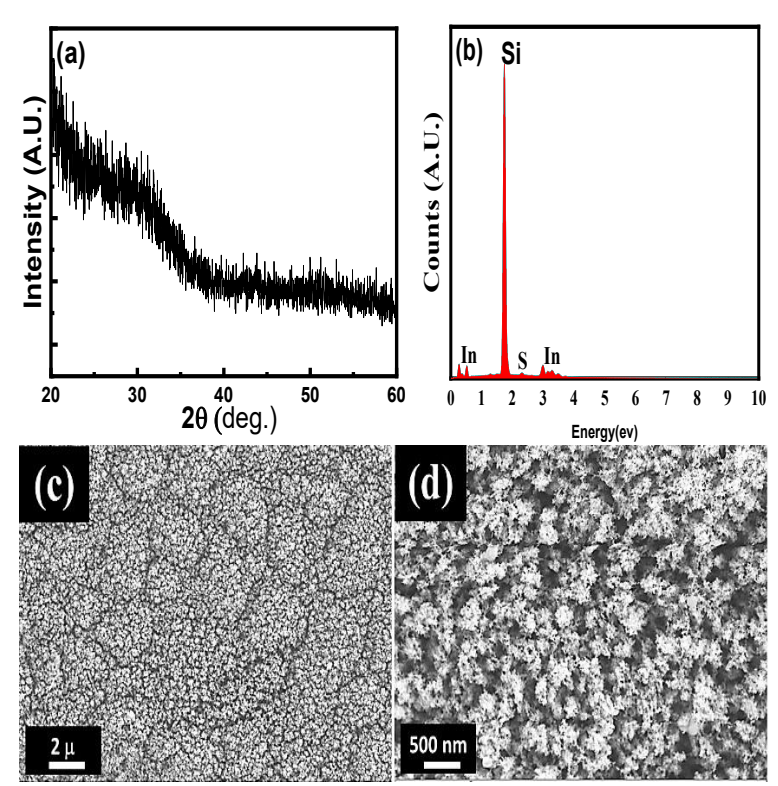


Fig.1. a) XRD pattern b) EDX spectrum, c) FE-SEM image at low magnification and d) FE-SEM image at higher magnification of In₂S₃ thin film.

3.2. Optical properties

3.2.1. Optical transmittance

The observed room temperature transmission spectrum is presented in Fig.2. The spectrum exhibits high optical transmittance (T) of >90%, which might be due to the poor crystallinity of the film. The result obtained in this study shows good agreement with previously work of Zhong et al. For $\rm In_2S_3$ thin films (645–680 Å) in thickness, deposited on glass substrates using thermal evaporation technique [18].

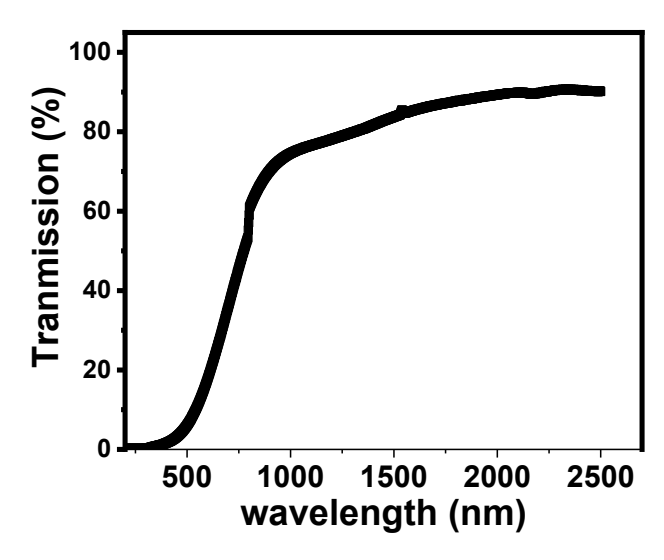


Fig.2. Optical Transmittance of In₂S₃ thin film.

3.2.2. Optical energy gap of In₂S₃ thin film

The measured absorbance, transmittance and reflectance values of deposited In_2S_3 films are utilized to estimate several optical constants, such as the extinction coefficient (K_{ex}), refractive index (n), absorption coefficient (α), optical band gap (E_g) and Urbach energy (E_U). The optical absorption coefficient (α) was estimated by optical transmission T(%) and reflection R(%) spectra using the following relation[19]:

$$\alpha = \frac{-1}{t} Ln \left[\frac{T}{(1-R)^2} \right] \tag{1}$$

In which, α , t, T, and R are the absorption coefficient, the thin film thickness (nm), transmission and reflection, respectively. Based on this relation, the absorption coefficient was evaluated in the high absorption region to obtain an accurate determination of the optical band gap energy. The optical band gap (E_g) of the film can be obtained by using the following relation:

$$\alpha h \nu = A(h\nu - Eg)^p \tag{2}$$

where A is a constant, h is the Planck constant, ν is the frequency and the exponent p characterizes the nature of band transition. The exponent p is a value that relies on the nature of transition $(p = \frac{1}{2} \text{ for direct allowed transition}, p = 2 \text{ for indirect allowed})$ transition and p = 3/2 for direct forbidden transition) [20]. $(\alpha h v)^2$ vs. hv plots (Tauc's plots) of the thin film is depicted in Fig.3. The bandgap energy of the In₂S₃ thin film was found from the intersection point as 2.34 ± 0.00468 eV. The E_g value is slightly higher than the band gap of In₂S₃ bulk (2.1-2.3 eV)[18]. The slightly higher value can be attributed to the amorphous nature or the quantum confinement effect due to the tiny size of the particles of deposited In₂S₃ thin film. Noteworthy, much higher E_g value (3.82 eV) was reported by Zhong et al. [18] for In₂S₃ thin film deposited using thermal evaporation technique. On the other side, Hashemi et al. reported E_g values between (2.05–2.12 eV) for In₂S₃ thin films deposited by chemical spray pyrolysis method using different In-salts as precursors [21].

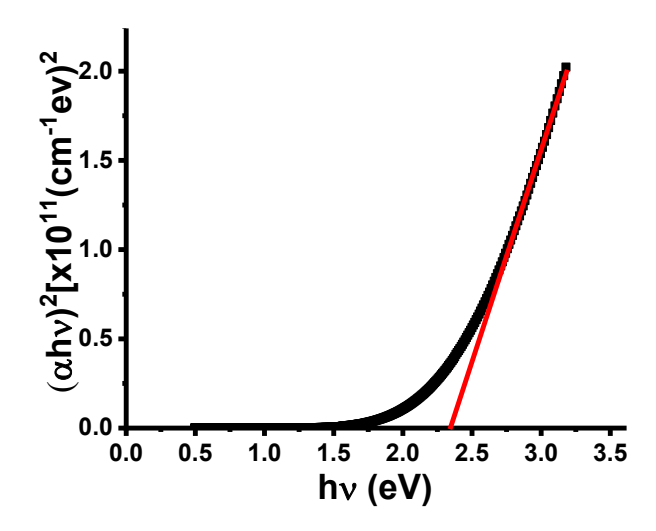


Fig.3. Optical band gap ((αhv)2 vs. hv) plot of In2S3 thin film.

3.2.3. Complex refractive index of In₂S₃ thin film

The complex refractive index of the In_2S_3 thin film can be expressed as $n^* = n + ik$, where the real part n represents the refractive index and the imaginary part k corresponds to the extinction coefficient.

The refractive index (n) is one of the most significant optical parameters for optoelectronic applications, as it provides essential information regarding the efficiency and performance of optical materials. The refractive index of the thermal evaporated thin film was estimated from the measured optical reflectance $R(\lambda)$, transmittance $T(\lambda)$ spectra and thin film thickness t using the following relation[22]:

$$n = \frac{1+R}{1-R} + \sqrt{\frac{4R}{(1-R)^2} + \left(\frac{\lambda}{4\pi t} \ln\left(\frac{(1-R)^2}{T}\right)\right)^2}$$
 (3)

The refractive index dependence on the wavelength for In_2S_3 thin film is shown in Fig.4. The refractive index increases at UV region of the spectrum and decreases sharply with the increase of wavelength. Also Herve and Vandamme(H–V) proposed another theoretical model to calculate the refractive index, which correlates the optical band gap energy (E_g) with refractive index (n), expressed as [23]:

$$n^2 = 1 + \left(\frac{A}{B + E_g}\right)^2 \tag{4}$$

Here, A and B are constants having values of 13.6 eV and 3.4 eV respectively. Specifically, A corresponds to the ionization energy of hydrogen atom, providing fundamental physical basis, and B is the empirically optimized parameter related to electron affinity[24] and E_g is the optical band gap energy. The refractive index value was found theoretically to be 2.57, which agrees well with the experimentally obtained value for as the deposited film.

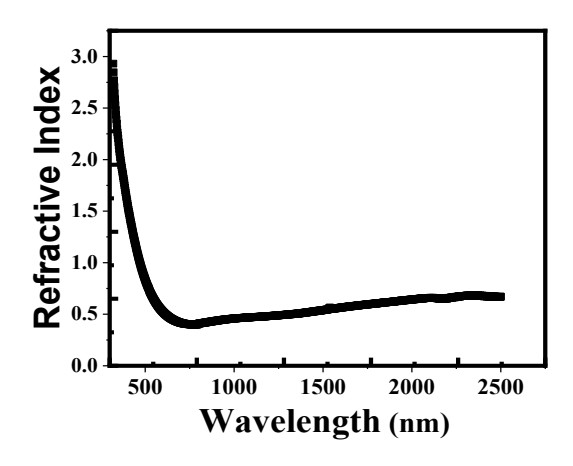


Fig.4. Variation of Refractive Index with the wavelength for In₂S₃ thin film

In the region of the fundamental absorption, the extinction coefficient (K_{ex}), accounts for the total optical losses in the material, arising from both absorption and scattering of the electromagnetic wave. The value of K_{ex} was calculated using the following relation[25]:

$$K_{ex} = \frac{\alpha \lambda}{4\pi} \tag{5}$$

Fig. 5. shows the variation of extinction coefficient as a function of wavelength. It is clear that the absorption index is low due to high optical transmittance and non-crystallinity of the thin film.

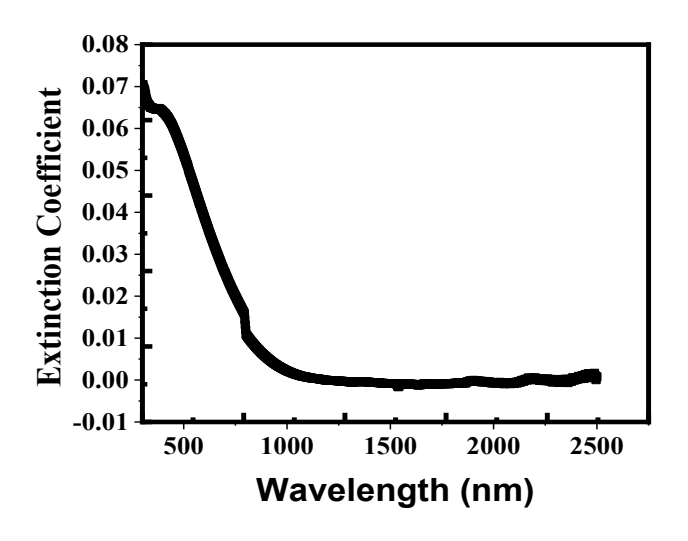


Fig.5. Variation of the extinction coefficient with the wavelength for In₂S₃ thin film

3.2.4. Urbach energy gap of In₂S₃ thin film

The spectral dependence of the logarithmic of optical absorption coefficient (α) vs incident energy (hv) in the low photon energy range was first discussed and studied for different semiconductors by Urbach and an empirical formula that correlates the $\ln(\alpha)$ with hv through following relation[23].

$$\alpha = exp\left(\frac{h\nu}{E_U}\right) \tag{6}$$

Where $h\nu$ is the photon energy and E_U is the Urbach energy

which refers to the width of the exponential absorption edge. The Urbach energy is a representative parameter for the microstructural defects of the lattice that correlates with the band tails. Fig.6. shows the variation of $ln(\alpha)$ vs. hv for the In₂S₃ thin film. This plot corresponds primarily to optical transitions between occupied states in the valence band tail to unoccupied states at the conduction band edge. The E_U value was calculated and founded to be 0.41 ± 0.0036 eV (R²=0.99915). Such relatively high value of E_U reverses high content of localized sates and thus high level of defects in the deposited thin film.

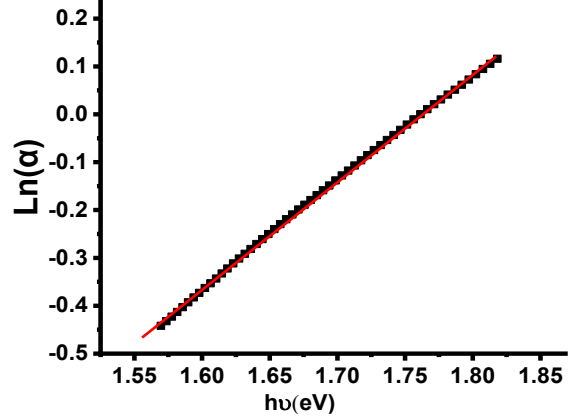


Fig.6. $Ln(\alpha)$ vs. hv of the deposited In₂S₃ thin film.

3.3 AC conductivity

Frequency (ω) dependence of the electrical conductivity (σ_t) for the In₂S₃ thin film, deposited on a glass substrate was measured within the frequency range (100 kHz - 8MHz) at different temperatures (303 -373 K) and the corresponding plots are depicted in Fig.7.a. The data imply that each plot comprises of two distinct regions: The DC region appears in low frequency range and shows a frequency-independent behavior that corresponds to the DC electrical conduction component σ_{dc} , where the DC conductivity (σ_{dc}) is very low (10⁻⁹ S/m), indicating a highly resistive behavior, but the AC region appears in high frequency range and shows a frequency-dependent behavior that corresponds to contribution of the AC conductivity (σ_{ac}) . σ_{ac} shows dispersion and frequency-dependent behavior, which is attributed to the hopping of charge carriers between localized states. The behavior in the high frequency region is found to be well represented by the Jonscher's universal power law [26]:

$$\sigma_{ac} = A\omega^s \tag{7}$$

where A is a proportionality constant, $\omega = 2\pi f$ is the angular frequency and s is the frequency exponent, which is a frequency dependent parameter [27]. The value of s provides insight into the dominant conduction mechanism. When $s \le l$, the conduction is typically governed by the correlated barrier hopping (CBH) model, in which the charge carriers hop between localized states over a potential barrier. In contrast, for s > l, the conduction may be attributed to large polaron hopping or Maxwell-Wanger interfacial polarization. The values of the s component were calculated from the $Log(\sigma_{ac})$ vs. ω (Fig. 7.b) plots and tabulated in Table 1. The calculated values are ranging between 0.9 and 1, indicating that the conduction mechanism is

Research Article

governed by the correlated barrier hopping (CBH) model. Similar results have been reported in previous studies on In₂S₃ thin films prepared by various deposition techniques. For instance, Seyam et al[17], Y. Bchiri et al [28] and Bouguila et al. [29] reported a clear conductivity-frequency plateau followed by a sharp increase in conductivity with frequency, and the behavior was attributed to charge carriers hopping in localized states. Furthermore, theoretical modeling by Abassi et al. [16] showed a clear transition from DC plateau to a pronounced high frequency dispersion behavior. These findings are in good agreement with the present study, reinforcing the dominance of the correlated barrier hopping (CBH) model. Noteworthy, it should be taken in consideration that the use of an insulating glass substrate could potentially induce interfacial polarization effects around the interface between the glass and the deposited film. However, the polarization inside the glass substrates primarily involves ionic polarization which can only occur at high frequencies specifically in the infrared region which is out of the scale of our measurements.

Dc conductivity analysis

The experimental data of dc conductivity were fitted using the Arrhenius expression. Fig.6(c) shows the extrapolated dc conductivity $\ln(\sigma_{dc})$ versus 1000/T plot of \ln_2S_3 thin film. The value of activation energy is calculated from the slope of the linear fit of $\ln(\sigma_{dc})$ vs 1000/T by using the Arrhenius equation[33]:

$$\sigma_{dc}(T) = \sigma_0 exp\left(\frac{-E_a}{K_B T}\right) \tag{8}$$
 Where σ_0 represents the pre-exponential factor, K_B is

Where σ_0 represents the pre-exponential factor, K_B is Boltzmann constant, and E_a denotes the activation energy of dc conduction and T is the temperature (K). as shown in fig.6(c), a good linear relationship between the ln (σ_{dc}) and $1000/\mathrm{T}$ is obtained. A small amount of energy 0.076 ± 0.0023 ev (R2 = 0.99349) is sufficient for the charge carriers to initiate the conduction process.

Temperature (K)	σ _{dc} x10 ⁻⁹	A x10 ⁻¹⁶	S
	(s/m)		
303	2.42 ± 0.125	1.36	1.0
313	2.46 ± 0.145	25.4	0.98
323	2.86 ± 0.154	36	0.97
333	2.90 ±0.162	38	0.96
343	3.33 ± 0.163	53	0.95
353	3.40 ± 0.177	83	0.93
363	3.83 ±0.233	86	0.92
373	4.11 ±0.203	148	0.90

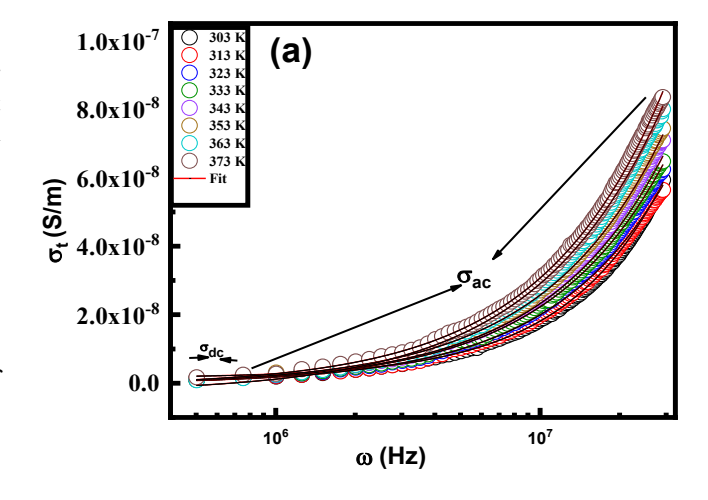
Table.1. The non-linear fitting extracted parameters of conductivity (σ_t) obeying the Jonscher power law for In_2S_3 thin film at different temperatures.

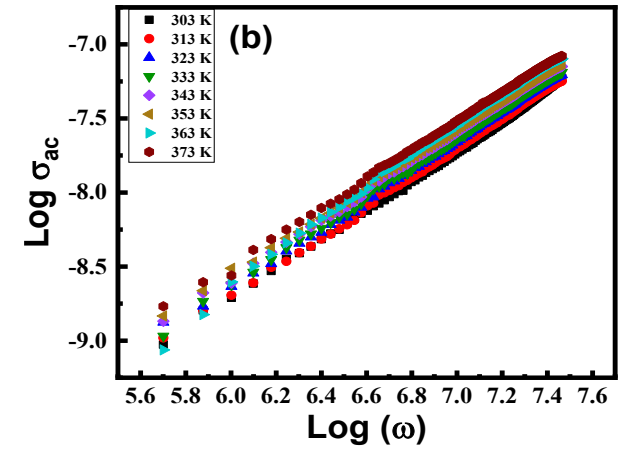
3.4 Dielectric Study

The dielectric behavior of materials is typically described using the complex permittivity (ε^*) [30]:

$$\varepsilon^* = \varepsilon' - j\varepsilon'' = \frac{\varepsilon}{\varepsilon_0} = \frac{C d}{\varepsilon_{0 A}}$$
(9)

Here, ε is the absolute permittivity, C is the measured capacitance, d is the thickness of the thin film, ε_0 is the permittivity of free space, A is the area of the thin film, ε' (the





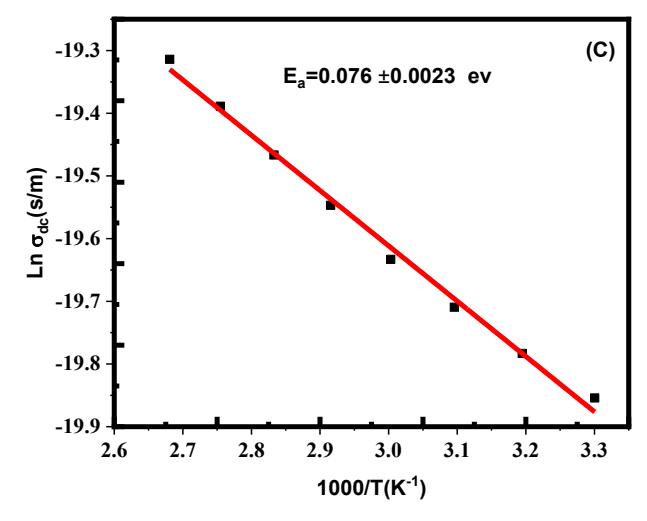


Fig.7. a) σ_t vs. ω plot, showing the non-linear fitting (red solid line) of conductivity (σ_t) obeying the Jonscher power law, b) $Log(\sigma_{ac})$ vs. $Log(\omega)$ and c) $Ln(\sigma_{dc})$ vs. 1000/T plot of In₂S₃ thin film at different temperatures.

real part of the permittivity) indicates the energy stored within the device due to polarization, while ϵ'' (the imaginary part) reflects the energy dissipated as heat. The real part ϵ' and the imaginary part ϵ'' of the complex permittivity can be expressed in terms of the loss angle δ :

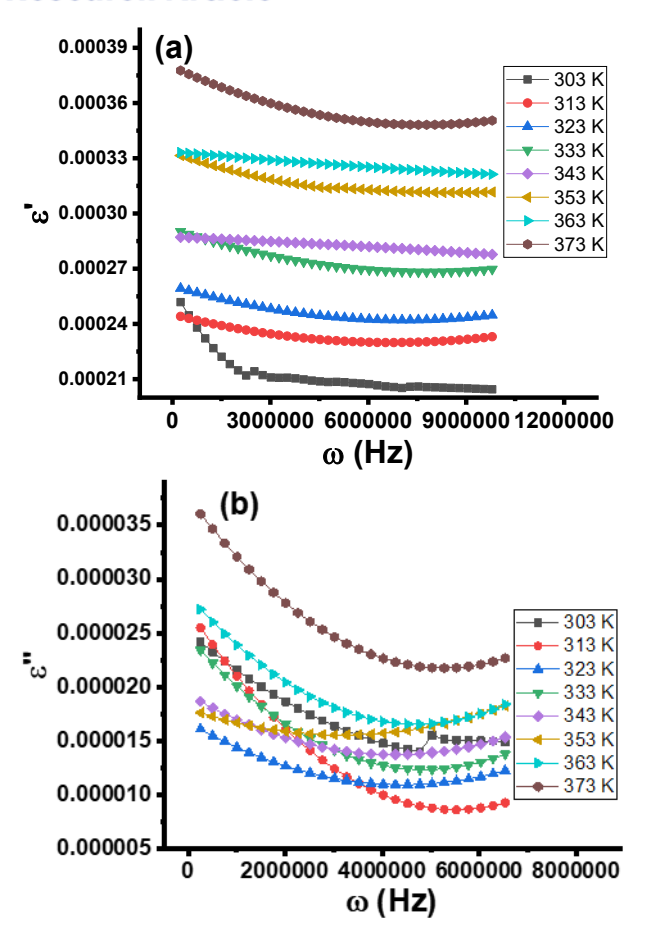


Fig.8. Frequency dependency of a) dielectric constant(ϵ ') and b) dielectric loss(ϵ ") of In₂S₃ thin film at different temperatures.

$$\varepsilon' = \varepsilon \cos \delta$$
 and $\varepsilon'' = \varepsilon \sin \delta$ (10)
The real and imaginary components of permittivity are connected via the dielectric loss tangent (tan δ) as follows[30]:
$$\varepsilon'' = \varepsilon' \tan \delta$$
 (11)

Real Part of Complex Permittivity (ε')

Fig. 8.a illustrates how the real permittivity ε' changes with frequency across different temperatures (ranging from 303 K to 373 K) for the deposited film. Generally, ε' decreases as frequency increases and eventually stabilizes at high frequencies. Furthermore, ε' increases with temperature. In polar materials, the total polarizability is a combination of different types of polarization: electronic, ionic, space charge, and orientational [31]. In our case, rotation direction polarization (RDP) and space charge polarization (SCP) are dominant, as electronic and ionic polarization are only active at very high frequencies (>1010 Hz). RDP arises at interfaces (e.g., grain boundaries) when an external electric field causes the rotation of many dipole moments due to defects. SCP results from trapped charges at these interfaces, forming dipoles. The In₂S₃ film exhibits a high dielectric constant, especially at low frequencies, and this value increases with temperature. This behavior is due to enhanced mobility of dipolar molecules at elevated temperatures, which makes them more responsive to the electric field, increasing overall polarization. At lower temperatures, however, the dipoles are less mobile and can't align easily with the field, limiting their contribution to ε' . Additionally, as temperature rises, bound dipoles acquire sufficient thermal energy to follow the oscillating field more effectively[31][30], thus contributing more to polarization and increasing ε' . Data from Fig.8.a confirm that ε' becomes nearly constant at higher frequencies. This is because, at these frequencies, dipoles can't follow with the applied field, so orientational polarization decreases, and only SCP (which is frequency-independent) remains significant[31][30].

Imaginary Part (Dielectric Loss, ε")

Fig. 8.b shows how the imaginary component ε'' varies with frequency across different temperatures. Typically, ε'' drops as frequency increases and shows relatively constant value at higher frequencies. Dielectric loss represents the energy dissipated (as heat) when an alternating electric field is applied, primarily due to the delayed response of the material to the external field. At lower frequencies, charge carriers can migrate more easily, contributing significantly to dielectric loss and leading to higher ε'' values. As frequency increases to intermediate levels, the impact of ion migration decreases, causing ε'' to decline. At high frequencies, dielectric loss arises mainly from ion vibrations, resulting in minimal and nearly stable ε'' values[31][30] .The data also show that ε'' rises with increasing temperature. Dielectric loss generally results from conduction, dipole, and vibrational mechanisms. As temperature increases, more charge carriers are released, enhancing conductivity and thereby increasing conduction-related losses.

4. Conclusion

In₂S₃ thin films were grown successfully by using vacuum thermal evaporation technique, resulting in an amorphous film with nanometric surface morphology and high optical transmittance. Structural characterization confirmed the absence of crystalline phases, while optical studies revealed a direct band gap of 2.34 ± 0.00468 eV, a significant Urbach energy of $0.41 \pm$ 0.0036 eV, indicating a considerable structural disorder and a density of localized states. the optical constants, refractive index and extinction coefficient were also evaluated. AC conductivity measurements demonstrated a frequency and temperature dependent behavior, with conduction dominated by the correlated barrier hopping (CBH) mechanism. The dc conductivity dominates the conduction mechanism at the lower frequency and supports the space charge polarization. Dielectric analysis confirmed enhanced dielectric constant and loss with increasing temperature, attributed to space charge and dipolar polarization effects. These results highlight the suitability of In₂S₃ thin films for use in dielectric and optoelectronic devices, particularly where high transparency and tunable electrical behavior are desirable.

CRediT authorship contribution statement:

Author Contributions: For research articles with several authors, a short paragraph specifying their individual contributions must be provided. The following statements should be used "Conceptualization, B.Y. and E.M.M.; methodology, E.K.S.

and M.S.K.; software, M.K and E.K.S.; validation, E.M.M., M.K. and M.B.Z.; formal analysis, A.A.A; investigation, B.Y; resources, B.Y and A.A.A.; data curation, M.K.; writing—original draft preparation, B.Y; writing—review and editing, E.M.M.; visualization, B.Y and M.S.K.; supervision, E.M.M. and M.K; project administration; M.K.; funding acquisition, B.Y. and E.M.M. All authors have read and agreed to the published version of the manuscript."

Data availability statement

The data used to support the findings of this study are available from the corresponding author upon request.

Declaration of competing interest

The authors declare that they have no known competing financial interests or personal relationships that could have appeared to influence the work reported in this paper.

Acknowledgments

This work was financially supported by the Academy of Scientific Research and technology (ASRT), Egypt, through the Next Generation Scientists Program (Cycle 7).

References

- [1] M. A. Mughal, R. Engelken, R. Sharma, Sol. Energy, 120 (2015) 131–146.
- [2] A. Timoumi, N. Bouguila, M. Chaari, M. Kraini, A. Matoussi, H. Bouzouita, J. Alloys Compd., 679 (2016) 59–64.
- [3] B. H. Kumar, M. C. S. Kumar, Mater. Sci. Semicond. Process., 111 (2020) 104 983.
- [4] J. Zhang, H. Wang, X. Yuan, G. Zeng, W. Tu, S. Wang, J. Photochem. Photobiol. C: Photochem. Rev., 38 (2019) 1–26.
- [5] P. Murahari, et al., Opt. Mater. (Amst)., 162 (2025) 116 903.
- [6] N. Barreau, Sol. Energy, 83 (2009) 363-371.
- [7] H. Spasevska, C. C. Kitts, C. Ancora, G. Ruani, Int. J. Photoenergy, 2012 (2012) 637 943.
- [8] E. Gnenna, N. Khemiri, M. Kanzari, J. Alloys Compd., 1021 (2025) 179625.
- [9] S. Rasool, G. Phaneendra Reddy, K. T. Ramakrishna Reddy, M. Tivanov, V. F. Gremenok, Mater. Today Proc., 4 (2017) 12491– 12495.
- [10] Y. Ji, et al., Surf. Coatings Technol., 276 (2015) 587–594.
- [11] R. V. Wagh, et al., J. Indian Chem. Soc., 102 (2025) 101810.
- [12] N. Barreau, A. Mokrani, F. Couzinié-Devy, J. Kessler, Thin Solid Films, 517 (2009) 2316–2319.
- [13] M. Sanchez-Tizapa, et al., Mater. Sci. Semicond. Process., 120 (2020) 105248.
- [14] R. J. Martín-Palma, A. Lakhtakia, Vapor-Deposition Techniques, Elsevier, 2013.
- [15] N. D. Sankir, M. S. Erkan Aydin, Int. J. Electrochem. Sci., 9 (2014) 3864–3875.
- [16] H. Abassi, N. Bouguila, A. Timoumi, J. Electron. Mater., 47 (2018) 2519–2525.
- [17] M. A. M. Seyam, A. E. Bekheet, A. Elfalaky, Phys. J., 104 (2001) 99–104.
- [18] Z. Y. Zhong, E. S. Cho, S. J. Kwon, Thin Solid Films, 547 (2013) 22–27.
- [19] C. Nefzi, M. Souli, N. Beji, A. Mejri, N. Kamoun-Turki, J. Mater. Sci., 52 (2017) 336–345.
- [20] X. Zhang, D. Zhang, X. Ni, H. Zheng, Solid State Electron., 52 (2008) 245–248.

- [21] M. Hashemi, et al., Sol. Energy, 215 (2021) 356-366.
- [22] C. Kumar, V. Kashyap, M. Shrivastav, F. Guzman, D. P. Singh, K. Saxena, Opt. Mater. (Amst)., 143 (2023) 114226.
- [23] S. Pathak, et al., Opt. Mater. (Amst)., 150 (2024) 115117.
- [24] P. Hervé, L. K. J. Vandamme, Infrared Phys. Technol., 35 (1994) 609–615.
- [25] R. Demir, F. Göde, E. Güneri, F. M. Emen, J. Mol. Struct., 1227 (2021) 129565.
- [26] Nature Publishing Group, Nature, 1977.
- [27] A. A. A. Darwish, M. M. El-Nahass, A. E. Bekheet, J. Alloys Compd., 586 (2014) 142–147.
- [28] Y. Bchiri, et al., Mater. Sci. Semicond. Process., 121 (2021) 105294.
- [29] N. Bouguila, I. Najeh, N. Ben Mansour, H. Bouzouita, S. Alaya, J. Mater. Sci. Mater. Electron., 26 (2015) 6471–6477.
- [30] H. A. A. Saadallah, et al., J. Mater. Chem. C, 12 (2024) 3739–3754.
- [31] M. P. Monis, et al., Ceram. Int., 50 (2024) 29081–29096.